Laser-Ablation Rates Measured Using X-Ray Laser Transmission

M. H. Edwards, D. S. Whittaker, G. J. Tallents, P. Mistry, and G. J. Pert
Department of Physics, University of York, York, YO10 5DD, United Kingdom

B. Rus, T. Mocek, M. Kozlová, J. Polan, A. Praeg, M. Stupka, and P. Homer
Department of X-ray Lasers, PALS Research Centre, Institute of Physics, Academy of Sciences of the Czech Republic, 182 21 Prague 8, Czech Republic

(Received 5 March 2007; published 9 November 2007)

The rate of laser ablation at irradiances of $\sim 2 \times 10^{14}$ W cm^{-2} of solid iron has been measured using the transmission of a neonlike zinc x-ray laser at 21.2 nm through thin iron targets. Ablated iron becomes transparent to the x-ray laser flux, enabling the thickness of unablated material and hence the rate of ablation to be measured from time resolved x-ray laser transmission.

DOI: 10.1103/PhysRevLett.99.195002 PACS numbers: 52.38.Mf, 52.38.Dx, 52.70.La

The efficiency of laser fusion will depend on the effectiveness with which laser energy is converted to the kinetic energy of implosion of a target. In "direct drive" laser fusion, visible or ultraviolet laser energy is absorbed in an expanding plasma "corona" up to the critical density for the laser light and the absorbed energy diffuses to the target surface and ablates solid material. The ablation of material towards the laser drives shock waves in the opposite direction into the target. A spherically symmetric geometry with an appropriate beam temporal profile is employed so that the shock waves coalesce and compress target material to the densities required for fusion reactions to occur [1–3]. The various steps in laser fusion (laser absorption, thermal conduction, ablation, shock wave formation, the achieving of spherical symmetry) have often been studied separately. Measurements associated with the steps have found applicability in a range of other applications of laser plasmas. For example, laser absorption and rates of ablation are important in the use of laser-plasmas in material coating and laser cutting [4].

The absorption fractions A in the interaction of laser radiation with solid targets have been determined by recording the fraction R of scattered and reflected laser light (and using $A = 1 - R$) or by employing plasma calorimeters to measure the kinetic energy of plasma expansion at some distance from the target [5,6]. With $\lambda = 1$ μm wavelength lasers, the absorption was found to be typically $A \approx 0.3$ at the irradiances of interest for laser fusion (10^{14}–10^{16} W cm^{-2}). The absorption fraction was found to increase with shorter wavelength ($\lambda < 0.5$ μm) driving lasers and decrease with longer wavelength ($\lambda > 1$ μm) lasers [5]. Higher wavelength lasers also absorb significant fractions of the laser energy into the heating of hot electrons with energies much greater than the thermal electron temperatures. Because of their long range and limited collisionality, hot electrons do not contribute directly to the ablation process [7].

Mass ablation rates arising when lasers irradiate solid targets have been previously measured by recording the time of emission from buried signature layers in the targets [8,9]. Ablation to the layer depth is said to be signaled by emission from the layer material, though such emission can also arise from an increase of electron temperature due to heat conduction without plasma expansion. Alternatively, mass ablation rates averaged over the laser pulse duration can be deduced from measurements of the total expanding plasma mass recorded from ion probe signals [10,11]. With longer pulse lasers, it is generally not feasible to determine ablation rates from the depths of craters left after laser irradiation as crater formation is often dominated by shock waves after the end of the laser pulse.

In this Letter we present measurements of temporally resolved laser ablation through thin targets of iron irradiated by an infrared laser using the transmission of a soft-x-ray laser at 21.2 nm directed normal to the target surface. Code calculations show that ablated hot iron plasma is close to fully transparent (Fig. 1) and so the x-ray laser

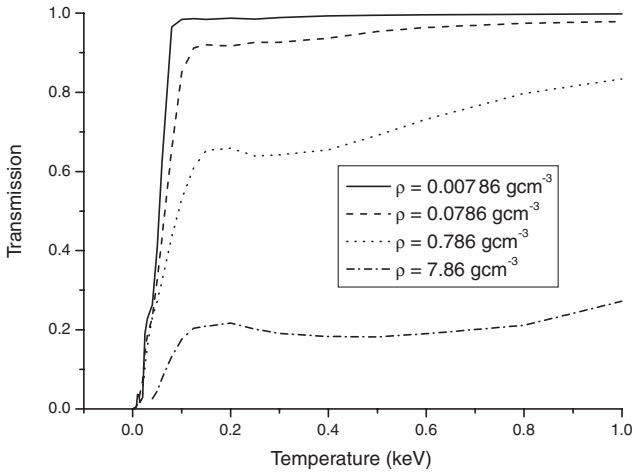

FIG. 1. The transmission at 21.2 nm as a function of temperature calculated by the TOPS code for iron at various densities ρ in g cm^{-3} (as indicated), but keeping the density-thickness product constant as for solid iron of 0.05 μm thickness.

transmission through an irradiated target is dominated by the absorption of the cold solid thickness of material not ablated. Our measurements differ from earlier studies with x-ray laser pulses probing spatial variations in transmission through thick foils associated with the Rayleigh-Taylor instability [12,13]. In these earlier probing studies, variations in x-ray laser transmission arose due to variations in opacity due to shock compression and areal density perturbations. We have also shown recently that if a transparent overcoat on a thin target is employed, the expansion of an opaque deeper iron layer is tamped and so the opacity of hot dense iron plasma is measured by recording the transmission of an x-ray laser [14].

The soft-x-ray laser at a wavelength of 21.2 nm arising from a $3p$-$3s$ transition in Ne-like zinc was produced using the PALS infrared (1.315 μm) laser operating with 480 ps duration output pulses [15]. The x-ray laser was created by irradiating a solid zinc target of length 3 cm with a low energy ($<$2 J) pulse focussed to a 500 microns wide line, followed 10 ns later by the main pulse of 400 J, focused to a line of width 100 μm. The long scale length preplasma with which the main pulse interacts provides good conditions for gain by reducing refraction effects, optimizing the gain volume and maximizing the absorption of the pump laser [16]. To improve further the brightness, reproducibility and uniformity of the x-ray laser beam, a half cavity mirror was installed and the reinjection point of the beam was tuned to drive the laser emission further into saturation. Operating well into laser saturation, the x-ray laser output energy per pulse was reproducible to within $\pm$30%. Streak camera measurements indicate that the pulse duration of the x-ray laser pulse is 90–130 ps [17]. Other studies have shown that the frequency bandwidth of x-ray laser pulses is extremely narrow (such that $\Delta\nu/\nu < 10^{-4}$ [17]) and is more than an order-of-magnitude narrower than the bandwidth of individual absorbing lines in the probed plasma.

A near-normal incidence spherical multilayer mirror focused the x-ray laser beam onto the sample target in a spot of 1 mm diameter at normal incidence. Another spherical multilayer mirror imaged the sample target plane to a CCD detector (PI-MTE CCD camera) so that the footprint of focused x-ray laser beam at the sample target was recorded with 6$\times$ magnification and spatial resolution of 4 μm. The sample targets comprised 0.8 μm thickness of aluminum onto which was deposited a 50 nm thickness of iron. These targets were ablated using a third, separate 10 J, 480 ps laser pulse at 1.315 μm, focused to a 120 μm full-width at half maximum diameter spot in the laser near-field with an approximately constant central spatial peak in irradiance (over 50 μm diameter). The variation in time of this peak irradiance is shown on Fig. 2. The transmission of the x-ray laser pulse through the ablated target at the spatial position corresponding to the peak of the focussed infrared irradiance (averaged over an area $\approx$30 μm diameter) was measured by comparing the recorded x-ray laser flux with and without an ablated target on different shots. This enabled transmission measurements accurate to within approximately $\pm$30%, according to the reproducibility of the x-ray laser from shot to shot. The time of arrival of the ablating laser pulse was adjusted relative to the other laser pulses producing the x-ray laser and the relative timing measured with a Hamamatsu streak camera, allowing the sample target transmission and hence ablation to be probed in time (Fig. 2). Simulations predict that the x-ray laser pulse peaks $\approx$ 100 ps before the peak of the 480 ps pump pulse. This shift in timing is allowed for in Fig. 2. The error in this 100 ps shift is small compared to the temporal resolution of the measurement ($\approx$ x-ray laser pulse duration $\approx$90–130 ps).

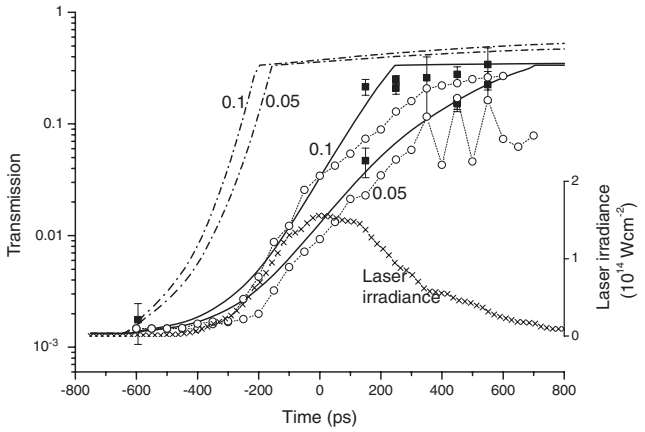

FIG. 2. Data points (filled squares) show the measured transmission of 21.2 nm laser light through 50 nm of iron and 0.8 microns thick aluminum as a function of time from the peak of a laser pulse of irradiance variation as shown (x) ablating the iron layer. Simulations of the transmission using EHYBRID and a postprocessor are shown as open circles with $A = 0.05$ or 0.1 (as labeled) absorption of the laser power controlled by altering the input laser energy. The solid and broken (dot-dash) curves are the transmission through unablated target material assuming ablation according to the deflagration model (broken curve) or self-regulating model (solid curve) with $A = 0.05$ or 0.1 (as labeled). For the self-regulating model, Li-like iron ionization is assumed.

Baffling was introduced to ensure there was no direct line of sight between the sample target and the CCD detector so that the contribution of self emission from the heated plasma arising in the sample target could be kept low. The recorded self emission was minimized further by installing a large pinhole ($\sim$500 μm in diameter) behind the sample target, close to the focal point of the x-ray laser beam. Comparing shots with and without the x-ray laser beam, self emission was found to be below the 10% level of the peak transmission of the x-ray laser at the CCD detector. The CCD detector was filtered using 0.16–2.86 μm thick aluminum foils.

The TOPS code developed at Los Alamos [18] can be used to model the opacity of iron and other material at high density and temperature. Figure 1 shows the TOPS evaluation of the transmission of a constant areal density of a layer of iron at the x-ray laser wavelength. The transmission increases rapidly with increasing temperature up to approximately 100–200 eV and then remains constant with further temperature increases. The transmission through the same areal density approaches unity at densities below 0.01 of the solid state density ($<7.86 \times 10^{-2}$ g cm^{-3}). This indicates that the transmission of the iron to the x-ray laser beam through the laser irradiated target works in a switchlike manner. As the outer layer of iron is ablated and has a lower density and higher temperature, its transmission becomes high compared with that of the remaining solid iron beneath. Consequently, the rate at which material is ablated can be observed by measuring the transmission of a target to the x-ray laser beam. The transmission at any particular time is dominated by the opacity of the cold unheated target at solid density ($T = 1.2 \times 10^{-3}$ for 50 nm solid iron on 0.8 μm thick aluminum and $T = 0.31$ for 0.8 μm thick solid aluminum), while the ablated plasma material at lower density is close to fully transparent.

A code similar to TOPS, but with temperatures, densities and time-dependent (non-LTE) ionization calculated by the EHYBRID fluid and atomic physics code has been developed [14,19]. Our absorption calculations are more accurate than TOPS as we use the fluid code time-dependent ionization calculation and utilize the spectral position and oscillator strength of approximately 25 000 lines tabulated by the Opacity Project [20] with line widths calculated using a modified semiempirical method assuming collisional broadening [21]. At the high densities where significant x-ray laser absorption occurs, the absorption predicted by our code is constant over the uncertainty range for the x-ray laser wavelength (21.202 ± 0.01 nm [22]) because of the large line broadening and high spectral density of absorbing lines. The predictions of the EHYBRID and opacity postprocessor code for our experiment are superimposed on Fig. 2. There is some oscillation in the simulated transmission on Fig. 2 due to oscillations in the computed ionization abundance and continuum lowering, but the simulated transmissions follow the experimental results and a simple ablation model (described below).

Using our EHYBRID and opacity postprocessor codes, we have examined x-ray laser transmission, $T = \exp(-\int \sigma \rho dx)$ as a function of distance x through our sample targets in order to check in more detail the switchlike nature of x-ray laser transmission as ablation occurs. For example, at time 120 ps after peak irradiance, transmission through the expanding iron plasma corona (here defined as density $\rho < 0.1$ g cm^{-3}) is 0.8. The transmissions through the "high density" (7.86 g cm$^{-3} > \rho >$ 0.1 g cm^{-3}) and solid ($\rho = 7.86$ g cm^{-3}) iron components are, respectively, 0.4 and 0.13. Our postprocessor code calculations show that the opacity σ of high density (7.86 g cm$^{-3} > \rho > 0.1$ g cm^{-3}) iron is comparable to the opacity of solid iron. For example, $\sigma = 6 \times 10^4$ cm^2 g^{-1} for solid iron, while $\sigma \geq 10^4$ cm^2 g^{-1} for iron of density 3 g cm^{-2} and temperature ≤ 50 eV.

Various analytic approximations with some small variations dependent on the precise assumptions have been developed for mass ablation rates when lasers irradiate solid targets. The most significant differences between models arise depending on whether laser energy is assumed dumped at the critical density or distributed throughout the coronal plasma. We will follow the scalings given by Pert [23]. The "deflagration" model [24] assumes that the laser energy absorption is localized at the critical density due to resonance absorption [25] or enhanced inverse bremsstrahlung with a constant plasma temperature downstream of the critical density towards the laser. The mass ablation rate $\frac{dm}{dt}$ (g cm^{-2} s^{-1}) depends on the absorbed irradiance, I_a (in W cm^{-2}) such that $\frac{dm}{dt} \approx 136 \rho_c^{2/3} I_a^{1/3}$, where ρ_c is the mass density (g cm^{-3}) at the critical density. If the heat release is distributed over the plasma corona due to inverse bremsstrahlung, the "self-regulating" model applies [26] and $\frac{dm}{dt} \approx 1.06 \times 10^{-5} \frac{A_m{}^{7/8}}{Z^{9/8}} \frac{I_a^{1/2}}{\lambda^{1/2} t^{1/4}}$, where A_m is the mass number of plasma material, Z is the average charge of the plasma where the laser is absorbed, λ is the laser wavelength (measured in μm here) and time t is measured from the onset of the laser pulse.

Using the deflagration and self-regulating models and considering the experimentally measured variation of laser irradiance with time incident onto the sample target (see Fig. 2), we calculate the target material ablated as a function of time and evaluate the transmission of the x-ray laser through the unablated target material using Ref. [27] (see model curves on Fig. 2). The deflagration and self-regulating models give different variations of the expected x-ray laser transmission and it is clear that the self-regulating model is applicable for this experiment with relatively long (480 ps) laser pulse irradiation. To fit the data, absorption (A), of the laser energy is a free parameter and is shown in the range $A = 0.05$–0.1 on Fig. 2. Such a value is low compared to $A \approx 0.3$ measured for lasers of wavelength 1.06 μm [5], but A is expected to be smaller for the conditions of this experiment, namely, a longer wavelength laser (1.315 μm). The variation in the experimental data points for Fig. 2 is thought to be associated with variation in laser absorption A over the range 0.05–0.1 from shot to shot as the variation is greater than our estimated measurement error.

A KAP ($2d = 2.6632$ nm) crystal spectrometer was used to record time-integrated measurements of plasma emission spectra from the ablated plasma. Spectra from

pure aluminum targets show that the "coronal" plasma was ionised to H-like and He-like ionization stages indicating that the electron temperatures exceeded $\approx$500 eV. Spectra from the targets coated with iron show Fe XXIV emission in the 0.79–0.86 nm range (see, for example, [28]) implying electron temperatures >600 eV [29]. At irradiance $I = 2 \times 10^{14}$ W cm^{-2}, we may expect a thermal electron temperature of $\approx$500 eV [30]. The plasma produced from the targets coated with iron do not show H- or He-like aluminum emission indicating that the 50 nm thickness of iron is not completely ablated during the laser pulse, in agreement with the x-ray laser transmission measurements for the self-regulating model with $A \leq 0.05$ (but not with the deflagration model). Cold aluminum K_α (0.834 nm) emission was observed with both pure Al and Fe coated Al targets. At $I\lambda^2 = 5 \times 10^{14}$ W cm^{-2}, we may expect a hot electron temperature of only $\approx$7 keV [5]. The presence of hot electrons is consistent with the low laser absorption ($A = 0.05$–0.1) to thermal plasma obtained in the fitting of the self-regulating ablation models to the x-ray laser transmission measurements.

We have also made x-ray laser transmission measurements similar to Fig. 2 for pure aluminum foils of 0.8 μm thickness ablated by 480 ps laser pulses. The transmission range is much narrower ($T = 0.31$–0.75) than for iron targets, but a self-regulating model of laser ablation again fits the experimental results. With aluminum, we could measure the x-ray laser transmission more accurately by using the transmission through unablated target material to calibrate the incident x-ray laser intensity for each individual shot. However, ablations rates can be determined with greater accuracy with material of high solid opacity such as iron, where, for example, for our experiment with 50 nm thickness of iron, we measure a transmission change due to ablation greater than 2 orders of magnitude.

In conclusion, laser ablation of solid iron targets has been temporally resolved using the transmission through sample target foils of a neonlike zinc x-ray laser at 21.2 nm. A self-regulating ablation model assuming 5%–10% laser energy absorption to thermal plasma fits the measured ablation rates. The rates of laser ablation of solid target materials are important in laser-fusion and laser material processing.

We acknowledge funding from the United Kingdom EPSRC, CCLRC, the MoD Joint Grants scheme, the Czech Science Foundation and EU Lasernet facility access.

[1] C. E. Max, C. F. McKee, and W. C. Mead, Phys. Rev. Lett. **45**, 28 (1980).
[2] S. Atzeni, Plasma Phys. Controlled Fusion **29**, 1535 (1987).
[3] S. E. Bodner *et al.*, Phys. Plasmas **5**, 1901 (1998).
[4] D. B. Chrisey and G. K. Hubler, *Pulsed Laser Deposition of Thin Films* (Wiley, New York, 1994).
[5] D. C. Slater *et al.*, Phys. Rev. Lett. **46**, 1199 (1981).
[6] D. F. Price *et al.*, Phys. Rev. Lett. **75**, 252 (1995).
[7] J. D. Hares, J. D. Kilkenny, M. H. Key, and J. G. Lunney, Phys. Rev. Lett. **42**, 1216 (1979).
[8] J. A. Tarvin *et al.*, Phys. Rev. Lett. **51**, 1355 (1983).
[9] P. A. Jaanimagi, J. Delettrez, B. L. Henke, and M. C. Richardson, Phys. Rev. A **34**, 1322 (1986).
[10] T. J. Goldsack, J. D. Kilkenny, and P. T. Rumsby, J. Phys. D **14**, L47 (1981).
[11] J. Grun, R. Decoste, B. H. Ripin, and J. Gardner, Appl. Phys. Lett. **39**, 545 (1981).
[12] E. Wolfrum *et al.*, Phys. Plasmas **5**, 227 (1998).
[13] D. H. Kalantar *et al.*, Phys. Rev. Lett. **76**, 3574 (1996).
[14] M. H. Edwards *et al.*, Phys. Rev. Lett. **97**, 035001 (2006).
[15] B. Rus *et al.*, Phys. Rev. A **66**, 063806 (2002).
[16] G. J. Tallents, J. Phys. D **36**, R259 (2003).
[17] P. Mistry, G. J. Tallents, and M. H. Edwards, Phys. Rev. A **75**, 013818 (2007).
[18] N. H. Magee, A. L. Merts, J. J. Keady, and D. P. Kilcrease, *The Los Alamos LEDCOP Code*, Los Alamos Report No. LA-UR-97-1038.
[19] D. S. Whittaker, M. H. Edwards, and G. J. Tallents, High Energy Density Phys. (in press).
[20] M. J. Seaton, Y. Yan, D. Mihalas, and A. K. Pradhan, Mon. Not. R. Astron. Soc. **266**, 805 (1994).
[21] M. S. Dimitrijevic and N. Konjevic, Astron. Astrophys. **172**, 345 (1987).
[22] J. Nilsen and J. H. Scofield, Phys. Scr. **49**, 588 (1994).
[23] G. J. Pert , Phys. Rev. A **75**, 023808 (2007).
[24] C. Fauquignon and F. Floux, Phys. Fluids **13**, 386 (1970).
[25] D. W. Forslund *et al.*, Phys. Rev. A **11**, 679 (1975).
[26] H. Puell, Z. Naturforsch. A **24**, 1807 (1970).
[27] http://www-cxro.lbl.gov/.
[28] B. C. Fawcett, A. Ridgeley, and T. P. Hughes, Mon. Not. R. Astron. Soc. **188**, 365 (1979).
[29] M. Arnaud and J. Raymond, Astrophys. J. **398**, 394 (1992).
[30] H. Nishimura *et al.*, Phys. Rev. A **23**, 2011 (1981).